


Photon-assisted tunneling resonantly extending the domain of the \mathcal{PT} -symmetric phaseL. Morales-Molina* and E. Aguilera-Valdés *Facultad de Física, Pontificia Universidad Católica de Chile, Casilla 306, Santiago 22, Chile*

(Received 24 May 2023; accepted 22 September 2023; published 9 October 2023)

We theoretically study the photon-assisted tunneling (PAT) in a \mathcal{PT} -symmetric triple-well potential (TWP) with balanced gain-loss between the noncentral wells and neutral central well. We show that the application of an ac drive in the central well permits to control the Rabi frequency of the population oscillation between the noncentral wells of the TWP. In particular, when a multiple of the driving frequency matches the chemical potential in the central well, an enhancement of the Rabi frequency is observed. Very importantly, we show that PAT resonantly extends the domain of the parameter space with a real spectrum. This is achieved for a gain-loss parameter well above its critical value in the nondriven case, which allows for stable Rabi oscillations in a strong gain-loss scenario. Moreover, within a Floquet framework, we find an analytical estimation of the critical gain-loss parameter for the different resonance values of the driving frequency. We also discuss possible physical realizations of our model.

DOI: [10.1103/PhysRevA.108.042205](https://doi.org/10.1103/PhysRevA.108.042205)**I. INTRODUCTION**

Among the most relevant transport quantum phenomena generated by the exchange of photons with the ac field is the photon-assisted tunneling (PAT) [1]. This is a resonant process that is known to be a powerful tool in the control of quantum tunneling [2]. Its study has been of significant importance for transport processes and hence for the development of nanodevices [3]. Its range of applications is very ample, encompassing areas such as semiconductor superlattices [4,5], coupled quantum dots [6,7], Josephson junctions [8], Bose-Einstein condensates in optical lattices [9–14], and photonic lattices [15,16].

Other areas with potential applications of PAT that remain largely unexplored are open systems. In this regard, non-Hermitian Hamiltonians with parity-time \mathcal{PT} reflection symmetry [17,18] may open new possibilities. These systems have been extensively investigated in the last two decades with applications in different research fields [19–44]. A main characteristic within systems with balanced gain-loss is the presence of a real spectrum when some real parameter γ that controls the degree of non-Hermiticity is below a critical value $\gamma_{\mathcal{PT}}$. It is, in fact, for the parameter domain $\gamma \leq \gamma_{\mathcal{PT}}$, that the system is at the exact \mathcal{PT} phase, otherwise the \mathcal{PT} phase is broken. Thus, motivated by the study of the \mathcal{PT} phases and their transitions, in recent years the research has been extended to setups subjected to ac fields [45–60]. An interesting example is the experimental observation of the parity-time-symmetric phase transition in dissipative Floquet systems which is achieved by tuning the amplitude and frequency of the ac drive [58,60].

The question that arises then is what happens when a resonant process such as the PAT phenomenon occurs in a system with balanced gain-loss? Can the PAT process be used to extend the domain of the \mathcal{PT} -symmetric phase in a system with

balanced gain-loss? If so, new applications could be conceived as, for example, in sensors [61], in which the resonances associated to the PAT would play a fundamental role.

To answer these questions, in the present work we consider a triple well potential (TWP) with balanced gain-loss between the noncentral wells and whose central well is neutral. We show that the application of an ac drive to the central well allows to control Rabi oscillations between the noncentral wells of TWP. In particular, we demonstrate that PAT largely enhances the frequency of Rabi oscillations when the system is at resonance with the ac drive. Very importantly, we find that PAT can resonantly extend regions with the real spectrum for relatively large values of the gain-loss parameter. These values can potentially be used for sensing purposes given the close relation between the resonant tunneling process and the stability of the Rabi oscillations.

The paper is organized as follows. In Sec. II, we describe the physical system and introduce the model with \mathcal{PT} -symmetric characteristics. In Sec. III, we first discuss the nondriven system where we analyze the conditions for the Rabi oscillations as well as its energy spectrum in the presence of balanced gain-loss. Then, we discuss the driven case. In particular, we analyze the enhancement in frequency of Rabi-like oscillations due to the PAT process. We demonstrate that PAT can resonantly extend stable regions with real spectrum for a value of the gain-loss parameter well above of its critical value in the nondriven case. To this end, we investigate regions with real Floquet quasienergies in phase diagrams created by the application of the ac drive. Finally, in Sec. IV, we summarize our results and discuss possible implementations for the findings described in the paper.

II. MODEL

We consider a triple-well with a balanced gain-loss between the noncentral wells and a neutral central well, which is sketched in Fig. 1. In this system the depth of the central well is different from the other adjacent wells, which creates

*Corresponding author: lmoralesl@uc.cl

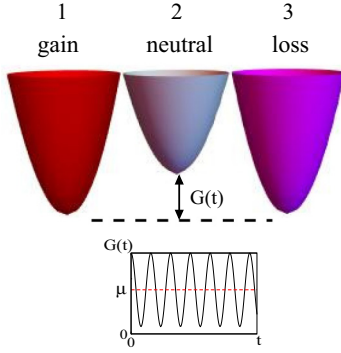


FIG. 1. Sketch of a triple well potential where the side wells experience balanced gain and loss whereas the central well is neutral. The central well is subjected to an ac drive given by the gate function $G(t)$, which is a periodic function shifted by a constant chemical potential μ . The numbers 1, 2, and 3 label the wells.

a chemical potential. We note that similar gain-neutral-loss setup can be seen in ferromagnetic trilayers [44] and in coupled ring cavities [39].

In addition to the static gain-neutral-loss setup, an ac drive is applied in the central well of the TWP that, together with the chemical potential, conform to the gate function $G(t)$ shown in Fig. 1. This is introduced to control the Rabi oscillations between the noncentral wells. In this regard, an analogous implementation of an ac field in a system of two ultrahigh-frequency oscillators with balanced gain-loss controlled by a time-dependent capacitance has been recently considered [58].

For the description of the tunneling dynamics inside of the TWP, we consider the tight-binding scenario, which reduces the analysis to the three-level model

$$i\dot{\psi}_1 = -\Omega\psi_2 + i\gamma\psi_1, \quad (1)$$

$$i\dot{\psi}_2 = -\Omega(\psi_1 + \psi_3) + G(t)\psi_2, \quad (2)$$

$$i\dot{\psi}_3 = -\Omega\psi_2 - i\gamma\psi_3, \quad (3)$$

where Ω is the tunneling rate between neighboring wells and γ is the gain-loss parameter. Here $G(t) = \mu + A \cos(\omega t)$ where μ is the chemical potential.

The equations above can be cast as the ac-driven Schrödinger equation

$$i\frac{\partial\Psi}{\partial t} = H\Psi, \quad (4)$$

where $\Psi = [\psi_1, \psi_2, \psi_3]^T$ and

$$\mathbf{H} = \begin{pmatrix} i\gamma & -\Omega & 0 \\ -\Omega & G(t) & -\Omega \\ 0 & -\Omega & -i\gamma \end{pmatrix}. \quad (5)$$

By defining the parity operator $\hat{\mathcal{P}}$, which interchanges 1 and 3 and the time reversal operator as $\mathcal{T} : i \rightarrow -i, t \rightarrow -t$, which reverses the time, it is easy to check that the Hamiltonian $\hat{H}(t)$ above fulfills the property $[\hat{\mathcal{P}}\hat{\mathcal{T}}, \hat{H}] = 0$. Thus, we can assert that this is a \mathcal{PT} -symmetric system. Interestingly, we note that \mathcal{PT} symmetry is preserved regardless of the chemical potential value. Furthermore, as we show below,

the fulfillment of the \mathcal{PT} symmetry in the presence of $G(t)$ allows the observation of stable Rabi oscillations due to a PAT process.

III. RESULTS AND DISCUSSION

The system of Eqs.(1) to (3) was investigated in the absence of both an ac drive and balanced gain-loss [62,63]. It was shown in Refs. [62,63] that the presence of a chemical potential can induce Rabi-like oscillations between the non-central wells of the TWP. Other studies in a similar static setup, in the presence of balanced gain-loss, focused their analysis on higher-order exceptional points [39,44]. As for the investigation of the PAT phenomenon, studies in a similar three-mode model have been carried out in the absence of balanced gain-loss and with the focus on the tunneling between adjacent modes [15,16]. Here, unlike these previous works, we investigate the role of PAT on the Rabi oscillations between the noncentral wells in the presence of balanced gain-loss with a neutral central well.

In the following we analyze the Rabi oscillations for the system of Eqs.(1) to (3) in the nondriven case.

A. Nondriven TWP

With no ac drive, the system of Eqs.(1) to (3) reduces to

$$i\dot{\psi}_1 = -\Omega\psi_2 + i\gamma\psi_1, \quad (6)$$

$$i\dot{\psi}_2 = -\Omega(\psi_1 + \psi_3) + \mu\psi_2, \quad (7)$$

$$i\dot{\psi}_3 = -\Omega\psi_2 - i\gamma\psi_3, \quad (8)$$

where $\Omega/\mu \ll 1$ is required for the existence of Rabi oscillations between the noncentral wells of the TWP as shown in Refs. [62,63] in the absence of gain and loss. Here, the presence of μ in Eq. (7) corresponding to the neutral well is key for stable Rabi oscillations. To gain insight, we look into the nondriven two-level model

$$i\dot{\psi}_1 = -\Omega\psi_2 + i\gamma\psi_1 + \frac{\mu}{2}\psi_1, \quad (9)$$

$$i\dot{\psi}_2 = -\Omega\psi_1 - i\gamma\psi_2 - \frac{\mu}{2}\psi_2, \quad (10)$$

where μ is a chemical potential that creates a bias between the two levels with balanced gain-loss. In this system, by interchanging 1 and 2 and applying the time-reversal operator $\hat{\mathcal{T}}$, one finds that the \mathcal{PT} symmetry is broken. Furthermore, from its corresponding eigenvalue equation $E^2 + \gamma^2 - \frac{\mu^2}{4} - i\gamma\mu - \Omega^2 = 0$, one obtains two solutions for E (eigenenergy) that are always complex with μ and γ distinct from zero. A similar result can be obtained in the system of Eqs. (6) to (8) by adding a constant energy difference between Eqs. (6) and (8).

Unlike the two-level system of Eqs. (9) and (10), in the system of Eqs. (6) to (8), a real spectrum can be found. For this purpose, we solve the secular equation of the system of Eqs. (6) to (8), from which we obtain the eigenvalue equation

$$E^3 - \mu E^2 + E(\gamma^2 - 2\Omega^2) - \mu\gamma^2 = 0. \quad (11)$$

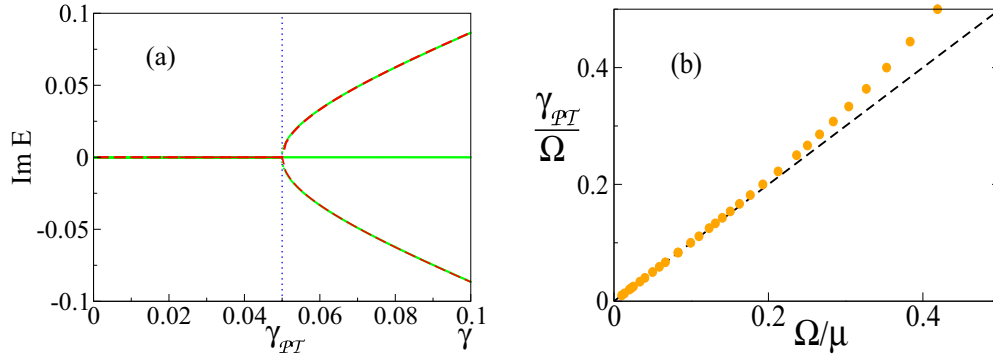


FIG. 2. (a) Imaginary values of the roots of Eq. (11) as a function of the gain-loss parameter γ . The red dashed line corresponds to the solutions of Eq. (14). The dotted line indicates the critical gain-loss parameter $\gamma_{\mathcal{PT}}$. $\Omega/\mu = 0.05$. (b) Critical gain-loss parameter $\gamma_{\mathcal{PT}}/\Omega$ as a function of the reciprocal value of the chemical potential Ω/μ . The black-dashed line corresponds to the analytical relation $\tilde{\gamma}_{\mathcal{PT}} = \frac{\Omega^2}{\mu}$.

First of all, for $\gamma = 0$, and taking into account $\Omega/\mu \ll 1$, one finds the eigenenergies $E_1 = -2\Omega^2/\mu$, $E_2 = \mu + 2\Omega^2/\mu$, and $E_3 = 0$ [62]. Given that $\mu \gg \Omega$, the oscillatory process of populations between the noncentral wells only involves the mode with eigenfrequency $2\Omega^2/\mu$, as we show below.

To analyze the gain-loss effects in the spectrum, we plot in Fig. 2(a), the imaginary values of the roots of Eq. (11) as a function of the γ . In this picture, one can observe that the energy spectrum becomes complex for values of γ larger than a critical value $\gamma_{\mathcal{PT}}$ at the so-called exceptional point. Here, to find the analytical value of $\gamma_{\mathcal{PT}}$ we resort to the adiabatic approach. Because $\Omega/\mu \ll 1$, ψ_2 rapidly approaches the value that is obtained from Eq. (7), so the adiabatic approach can be applied. Thus, by setting $\dot{\psi}_2 = 0$, one obtains

$$i\dot{\tilde{\psi}}_1 = -\tilde{\Omega}\tilde{\psi}_3 + i\gamma\tilde{\psi}_1, \quad (12)$$

$$i\dot{\tilde{\psi}}_3 = -\tilde{\Omega}\tilde{\psi}_1 - i\gamma\tilde{\psi}_3, \quad (13)$$

where $(\tilde{\psi}_1, \tilde{\psi}_3) = (\psi_1, \psi_3)\exp[-i\tilde{\Omega}t]$ and $\tilde{\Omega} = \frac{\Omega^2}{\mu}$.

These effective equations model a two-level quantum system with $\tilde{\Omega}$ as the characteristic Rabi frequency of the system. This system of coupled equations is known to fulfill the \mathcal{PT} symmetry whose eigenvalues are given by

$$\lambda_{\pm} = \pm\sqrt{\tilde{\Omega}^2 - \gamma^2}. \quad (14)$$

Hence for values of $\gamma > \tilde{\gamma}_{\mathcal{PT}} = \frac{\Omega^2}{\mu}$, the eigenvalues become complex. In Fig. 2(a), the imaginary values of Eq. (14) are superimposed to the exact imaginary spectrum of eigenenergies, showing a full agreement and thus predicting with great accuracy the critical value $\gamma_{\mathcal{PT}}$. To elucidate the validity region of the relation $\tilde{\gamma}_{\mathcal{PT}} = \frac{\Omega^2}{\mu}$, we show in Fig. 2(b), the numerical solutions of $\gamma_{\mathcal{PT}}/\Omega$ as a function of Ω/μ , together with $\tilde{\gamma}_{\mathcal{PT}} = \frac{\Omega^2}{\mu}$ that is depicted by a dashed straight line. Here, for values of $\Omega/\mu \ll 1$, where the adiabatic theory is applicable, the figure clearly shows a good agreement between the numerical results and the analytical prediction. On the other hand, for values of $\Omega \gtrsim 0.2\mu$, when the adiabatic condition is not satisfied, a deviation of the straight line is observed. Another interesting result from Fig. 2(b) is that $\gamma_{\mathcal{PT}}$ scales

inversely proportional to μ . This shows that \mathcal{PT} symmetry alone does not guarantee the existence of a real spectrum.

According to Eqs. (12) and (13), the population in the first well $|\psi_1|^2$ oscillates with two times the frequency of $\tilde{\Omega}$, which also holds for the population in the third well $|\psi_3|^2$ and its difference. In what follows, to characterize the coherent oscillatory process of populations between the noncentral wells, we define the population imbalance $z(t)$ as the population difference between the first and third wells, viz.

$$z(t) = |\psi_1|^2 - |\psi_3|^2, \quad (15)$$

which is a quantity that can be experimentally measured [64,65]. Here, the characteristic oscillation frequency of $z(t)$, given by the eigenfrequency $2\Omega^2/\mu$, serves as a benchmark for the ac-driven setup.

B. Driven TWP

The application of an ac drive can, in principle, modify the properties of the tunneling dynamics in the TWP. Let us first consider a vanishing gain-loss parameter, namely, $\gamma = 0$. We are interested in the analysis of Rabi coherent oscillations between the noncentral wells, when a gate function $G(t)$ is applied in the central well. In Fig. 3(a) are depicted coherent oscillations of the population imbalance $z(t)$ for different frequencies of the ac drive. In this figure we observe that the oscillation period can increase or decrease depending on the frequency ω of the ac drive. Particularly interesting are the cases whose driving frequencies differ by small values with a large difference between their oscillation periods. An example are the curves with $\omega = 10\Omega$ (red line) and $\omega = 12\Omega$ (blue line) depicted in the Fig. 3(a), where the oscillation period of the blue curve is approximately six times that of the red curve.

To gain some understanding, in Fig. 3(b) is featured the oscillation frequency of the population imbalance as a function of the ratio ω/μ . In this figure is also depicted with a red-dashed line the oscillation frequency of the nondriven case for comparison purposes. This value is reached in the figure for large values of the driving frequency, namely, for $\omega \rightarrow \infty$.

On the other hand, we are able to observe points with zero Rabi-oscillation frequency values. These correspond to situations where populations remain localized and tunneling

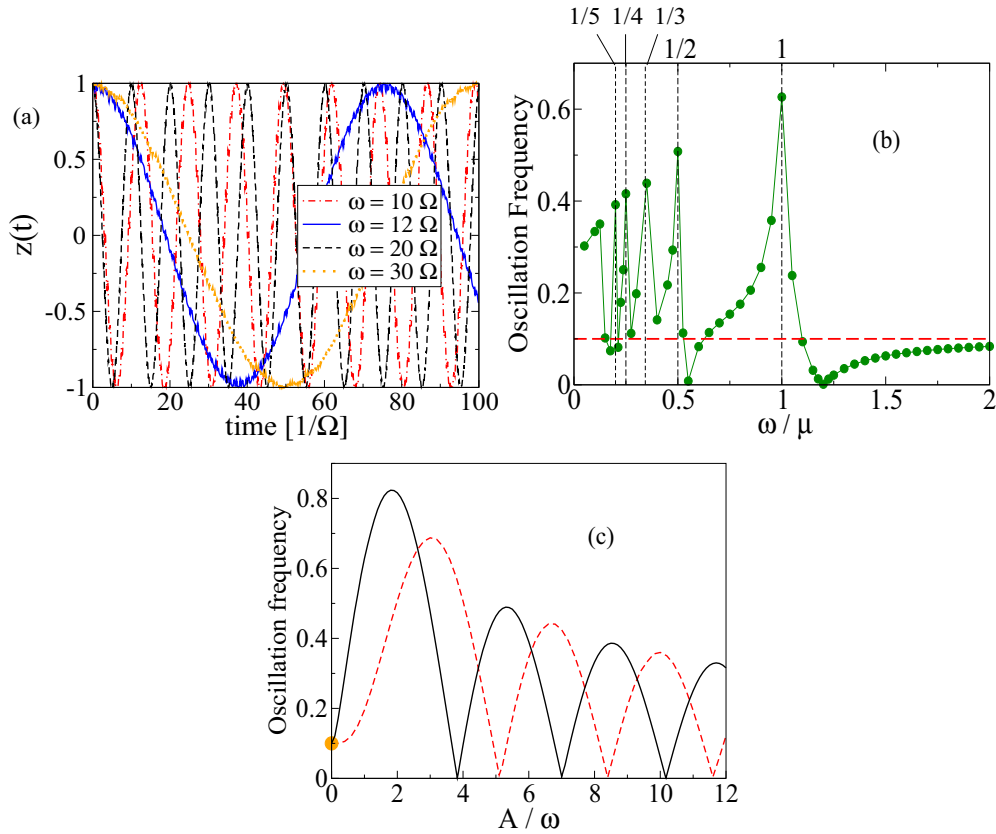


FIG. 3. (a) Population imbalance evolution for frequencies of the ac drive, $\omega/\Omega = 10, 12, 20, 30$. (b) Oscillation frequency of $z(t)$ (in units of Ω) as a function of the ratio ω/μ . The vertical black-dashed lines indicate the location of the resonance frequencies $\omega_m = (1/m)\mu$, with $m = 1, 2, 3, 4, 5$. The horizontal red-dashed line depicts the corresponding oscillation frequency 0.1Ω for $A = 0$. In both (a) and (b) $A = 20\Omega$. (c) Oscillation frequency of $z(t)$ (in units of Ω) as a function of the amplitude of the drive A/ω . (black-solid line) $\omega = \omega_1$; (red-dashed line) $\omega = \omega_2$, $\Omega/\mu = 0.05$. The orange dot with oscillation frequency 0.1Ω indicates the point with $A = 0$.

is fully suppressed, which is usually referred to as a coherent destruction of the tunneling (CDT) process. This is a phenomenon that has been largely addressed in the literature [2] and that we refer to later on.

A noticeable feature in Fig. 3(b) is the presence of peaks for values of the ac drive frequency ω that fulfill the resonance condition $m\omega_m = \mu$ with $m = 1, 2, \dots$. Note that, at the main resonance peak $\omega = \omega_1$, the oscillation frequency of the population imbalance is of the order of the tunneling rate Ω between neighboring wells. This enhancement in the frequency of the Rabi oscillation is a consequence of a photon-assisted tunneling process. Thus, when a multiple of the external frequency matches the chemical potential of the system, a resonant transfer of populations between the first and third wells takes place.

The phenomenon of PAT and its effect over the Rabi oscillations is also determined by the amplitude of the drive. To elucidate such a dependence, we show in Fig. 3(c) the behavior of the Rabi oscillation frequency as a function of the amplitude A/ω in a resonant scenario. In this figure are featured two curves corresponding to $\omega = \omega_1$ (black solid line) and $\omega = \omega_2$ (red-solid line). Both curves start from the predicted value $2\Omega^2/\mu = 0.1\Omega$ for $\mu = 20\Omega$. On the other hand, both curves show points with zero frequency values for the Rabi oscillations, which are associated to a CDT process. These points are the zeros of the $J_1(A/\omega)[J_2(A/\omega)]$ for the

black (red) curve, where J_1 and J_2 are the Bessel functions of first kind, as we show later on. Here, the large variation of the oscillation frequency with the amplitude of the ac drive could, in principle, allow a dynamic control of the frequency of the Rabi oscillations that take place between the noncentral wells of the TWP.

So far, we showed the enhancing effect of PAT on the frequency of Rabi oscillations in the absence of a balanced gain-loss, that is, for $\gamma = 0$. We now investigate the system when $\gamma \neq 0$. In particular, we are interested in the possible effect of PAT on the stability of Rabi oscillations for $\gamma \neq 0$. To gain insight, we resort to the Floquet formalism [2]. Within this framework the Floquet states can be expressed as

$$\tilde{\psi}_j(t) = \tilde{\psi}_j(t) \exp(-i\varepsilon_j t), \quad j = 1, 2, 3, \quad (16)$$

where ε_j are the quasienergies and $\tilde{\psi}_j(T + t_0) = \tilde{\psi}_j(t_0)$. Here, the quasienergies defined as $\varepsilon_j = \text{Re}(\varepsilon_j) + i\text{Im}(\varepsilon_j)$ [53] with $j = 1, 2, 3$, are the eigenvalues of a time-independent matrix \mathbf{R} , which is connected to the monodromy matrix \mathbf{M} of Eqs. (1) to (3) through the equation

$$\mathbf{M} = e^{-i\mathbf{R}T}. \quad (17)$$

So, by diagonalizing \mathbf{M} , we get the quasienergies of the system. In Fig. 4, we show in a phase diagram, the imaginary values of the complex Floquet spectrum as a function of the

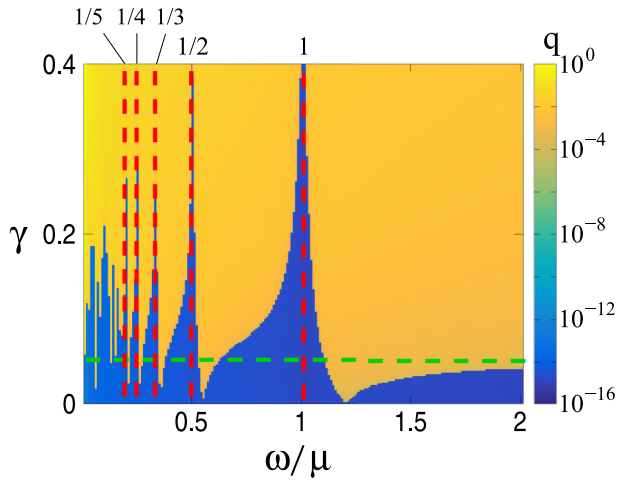


FIG. 4. Phase diagram for the normalized ac frequency ω/μ and gain-loss parameter γ (in units of Ω). The plot shown is the maximum of the imaginary part of the quasienergy spectrum ($q = \max[\text{Im}(\varepsilon)]$). The horizontal green dashed line corresponds to the critical gain-loss parameter $\gamma_{PT} = 0.05\Omega$ for $A = 0$. The vertical red-dashed lines indicate the location of the resonance frequencies $\omega_m = (1/m)\mu$ with $m = 1, 2, 3, 4, 5$; for a fixed chemical potential. The other parameters are $A/\omega = 1$ and $\Omega/\mu = 0.05$.

driving frequency ω and the gain-loss parameter γ . In this phase diagram, the regions in blue (yellow) correspond to vanishing (nonzero) imaginary values of all quasienergies (ε_j with $j = 1, 2, 3$). Also depicted with a green-dashed line is the analytical value $\gamma_{PT} = 0.05\Omega$ of the critical gain-loss parameter with $A = 0$ whose value is reached in the figure for large values of the driving frequency, namely, for $\omega \rightarrow \infty$.

The phase diagram also shows narrow stripes of the real spectrum for relatively large γ at the resonance frequencies ω_m with $m = 1, 2, \dots$. It is at these frequencies that peaks with large Rabi frequencies appear as a result of the PAT process, as shown in Fig. 3(b). This shows a clear connection between the PAT process and large extensions of the parameter space with real spectrum. Here, the existence of narrow stripes with real spectrum at the frequencies ω_m may provide a tool of high sensitivity for the detection of small fluctuations in the chemical potential, which could be exploited for sensing purposes [61,63].

In view of the significant extension of the parameter space with real spectrum due to the PAT, we calculate below analytical expressions of the critical gain-loss parameter for the resonance frequencies ω_m , with $m = 1, 2, \dots$. To this end, and for the sake of convenience, we resort to the high-frequency regime. In this regime, the equations are averaged over the period of the drive allowing to get some effective equations with rescaled parameters.

The time average is valid provided $\Omega \ll \max[\omega, \sqrt{A\omega}]$ [52]. So, by making the transformation

$$\psi_1(t) = \phi_1(t), \quad (18)$$

$$\psi_2(t) = \phi_2(t)e^{-i\left[\frac{A}{\omega}\sin(\omega t) + m\omega t\right]}, \quad (19)$$

$$\psi_3(t) = \phi_3(t), \quad (20)$$

and averaging over the period of the drive, we find

$$i\dot{\phi}_1 = i\gamma\phi_1 - \Omega Q\phi_2, \quad (21)$$

$$i\dot{\phi}_2 = -\Omega Q(\phi_1 + \phi_3), \quad (22)$$

$$i\dot{\phi}_3 = -i\gamma\phi_3 - \Omega Q\phi_2, \quad (23)$$

where $Q = (-1)^m J_m$. Here, $J_m = J_m(A/\omega)$ with $m \geq 1$ is the m th order of the Bessel function of the first kind [66]. By diagonalizing the Hamiltonian matrix of the system of Eqs.(21) to (23), we find the quasienergies

$$\varepsilon_{1,2} = \pm\sqrt{2\Omega^2 J_m^2 - \gamma^2}, \quad (24)$$

and $\varepsilon_3 = 0$.

Thus, from Eq. (24) we get for the resonance frequency ω_m , the critical gain-loss parameter

$$\gamma_{PT}^{(m)} = \sqrt{2}\Omega|J_m|. \quad (25)$$

Hence, when $\gamma > \gamma_{PT}^{(m)}$, the spectrum becomes complex. Interestingly, $\gamma_{PT}^{(m)}$ vanishes at the zeros of J_m .

It is worth noting that a similar finding can be obtained by applying an ac driving, as proposed in Ref. [56], to the two-level system of Eqs. (9) and (10). For this case, following similar steps as above, one obtains the critical gain-loss parameter $\Omega|J_m|$, which is smaller than $\gamma_{PT}^{(m)}$. In that regard, a larger extension of the real spectrum is achieved with the triple-well setup.

Let us now check the validity of Eq. (24). So, let us first consider the case $\gamma = 0$. In Fig. 5(a), we show the behavior of the quasienergies as a function of the amplitude of the ac drive with $\omega = \omega_1$. In this plot, the analytical values of Eq. (24) with $m = 1$ appear superimposed over the numerical results, showing an excellent agreement for most of the spectrum. In particular, we note that at the zeros of the Bessel function $J_1(A/\omega)$ with $A/\omega = 3.8317; 7.0156; \dots$; the quasienergies cross, leading to a CDT with null oscillation frequency as shown in Fig. 3(c). Equation (24), however, does not fulfill the behavior observed for values of the amplitude close to zero, as expected from the averaging condition. Instead, in the limit $A/\omega \rightarrow 0$, the curves approach some finite energy values. These values are associated to the energies of the nondriven system $-\frac{2\Omega^2}{\mu}$ and $\mu + \frac{2\Omega^2}{\mu}$. Note that, at the frequency $\omega = \omega_1$, the width of the Floquet-Brillouin zone is the chemical potential, meaning that absorbing a photon compensates for the displacement of μ between the quasienergy $\frac{2\Omega^2}{\mu}$ and eigenenergy $\mu + \frac{2\Omega^2}{\mu}$.

Let us now look into the case when $\gamma \neq 0$. In Fig. 5(b) we show in the upper and lower panels the respective real and imaginary values of the quasienergies as a function of the amplitude A for $\gamma = 0.1\Omega$. In the upper panel, we observe that real values of quasienergies, in the vicinity of crossing points, merge at exceptional points (EPs). In these EPs the quasienergies become complex with no vanishing imaginary part. As a result, for complex quasienergy values the system is unstable, meaning that an uncontrollable growth of the amplitude of the Rabi oscillations takes place.

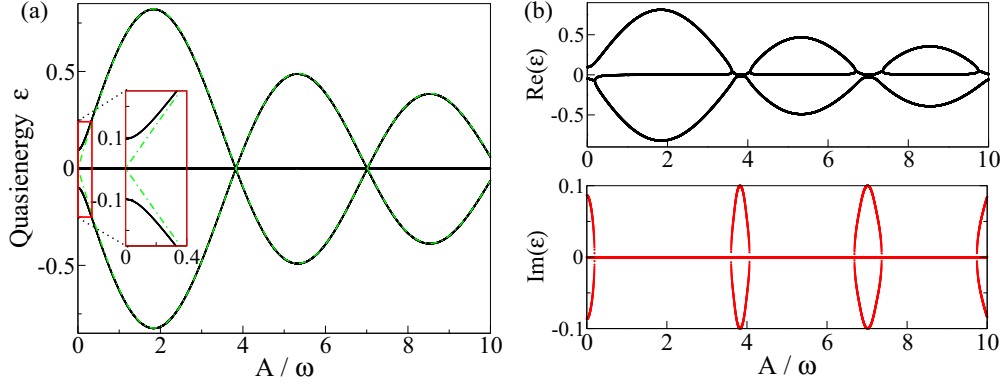


FIG. 5. (a) Quasienergy ε versus amplitude A/ω of the ac drive for $\gamma = 0$. The black-solid lines correspond to numerical solutions whereas green dashed lines correspond to solutions given by Eq. (24) with $\gamma = 0$. Inset shows an enlargement of the figure in the vicinity of $A = 0$. (b) Complex quasienergy spectrum as a function of the amplitude A for $\gamma = 0.1\Omega$. The upper and lower panels correspond to the real and imaginary components of the quasienergy ε . The other parameters are $\omega = \mu = 20\Omega$.

By looking into Fig. 5(b), and comparing with Fig. 3(c) for $\gamma = 0$, one can deduce that complex quasienergies emerge for amplitudes of the drive where the Rabi-oscillation frequency is low. This implies that at the zeros of the Bessel function J_1 the population imbalance with $\gamma > 0$ is not longer stable.

In general, and as predicted by Eq. (24), quasienergies become complex when the gain-loss parameter γ exceeds the critical value $\gamma_{\mathcal{PT}}^{(m)}$ given by Eq. (25). Thus, to corroborate this prediction, we show in a phase diagram for A and γ the regions with vanishing (blue) and nonzero imaginary values (yellow) of the quasienergies (see Fig. 6). The left panel corresponds to the case $\omega = \omega_1$, whereas in the right panel is featured the situation $\omega = \omega_2$. In these panels, regions with a real spectrum have a lobe shape. Importantly, the lobes have critical values of γ larger than $\gamma_{\mathcal{PT}}$, the corresponding critical value for the nondriven case. This means that the action of the ac drive extends the real spectrum beyond the nondriven scenario, thus having a stabilization effect on the Rabi oscillations. In the phase diagram are depicted with solid gold lines the analytical values $\gamma_{\mathcal{PT}}^{(m)}$ for $m = 1$ and $m = 2$ in the left and right panels, respectively. In both panels the border

of the regions with real spectra are reasonably well described by $\gamma_{\mathcal{PT}}^{(m)}$ values, reaching perfect agreement at the zeros of the corresponding Bessel functions J_m , except when $A/\omega \rightarrow 0$. In the case of $A = 0$, the numerical values in both panels feature the same critical finite value $\gamma_{\mathcal{PT}} = 0.05\Omega$ which is in full agreement with the estimated $\gamma_{\mathcal{PT}} = \frac{\Omega^2}{\mu}$ for $\mu = 20\Omega$. Furthermore, excluding the points near $A/\omega = 0$, we note that the curves of $\gamma_{\mathcal{PT}}^{(m)}$ values in Fig. 6 show an exact behavior to the Rabi frequency curves depicted in Fig. 3(c). Interestingly, we observe that $\gamma_{\mathcal{PT}}^{(m)}$ becomes larger as the Rabi frequency increases, which means that the transfer rate of populations between the noncentral wells plays a fundamental role in the stability of the system. A physical explanation to this phenomenon could be attributed to the fact that a faster transfer of populations between the wells can eliminate more rapidly the excess of population generated in the first well by transferring it to the third well where losses occur, thus preventing an uncontrollable growth of the population imbalance $z(t)$.

The above results shed light on the resonantly extended regions with \mathcal{PT} phase and provide a good foot for their

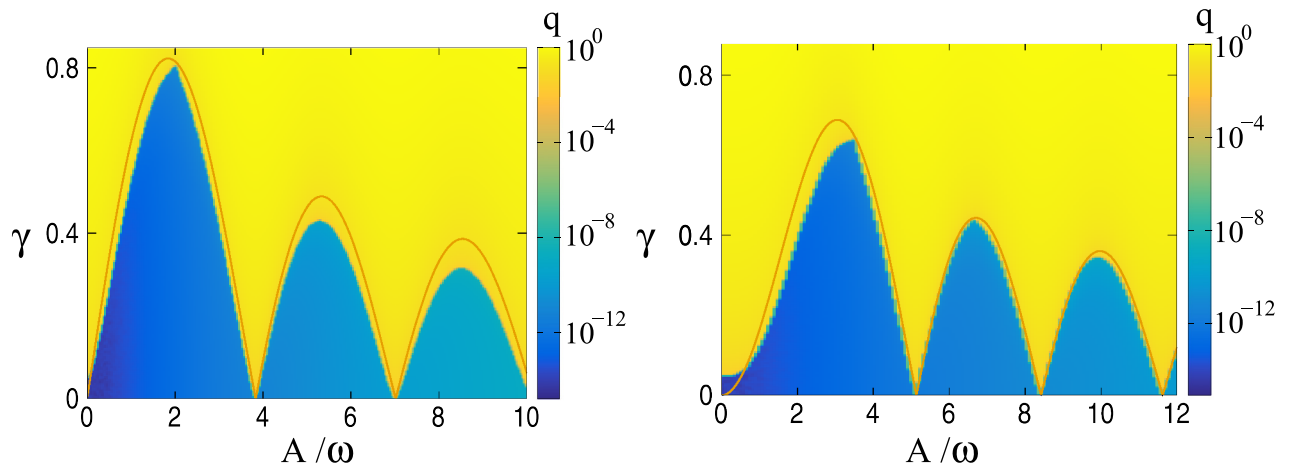


FIG. 6. Phase diagrams for the amplitude A/ω and gain-loss parameter γ (in units of Ω). In both panels, the plot shown is the maximum of the imaginary part of the quasienergy spectrum ($q = \max[\text{Im}(\varepsilon)]$). Left panel: $\omega = \omega_1 = \mu$. Right panel: $\omega = \omega_2 = \mu/2$. Both panels are depicted with solid gold lines $\gamma_{\mathcal{PT}}^{(m)}$ from Eq. (25) with $m = 1$ and $m = 2$ for the left and right panels, respectively. The parameter $\Omega/\mu = 0.05$.

implementation in systems with a gain-neutral-loss setup where the central element is under the presence of an ac field.

IV. CONCLUDING REMARKS

We studied the photon-assisted tunneling in a \mathcal{PT} -symmetric triple-well potential with balanced gain-loss between the noncentral wells and neutral central well. We first showed that using the ac field allows to control the frequency of Rabi oscillations between the noncentral wells. In particular, when the frequency of the drive matched the chemical potential in the central well, an enhancement of the Rabi-frequency oscillations could be observed, which is an indication of a photon-assisted tunneling process. Very importantly, we investigated in detail, analytically and numerically, the effect of the frequency and the amplitude of the ac drive on the position of the exceptional point of the system. As a relevant result, we found that photon-assisted tunneling can resonantly extend regions of the parameter space with a real spectrum for a value of the gain-loss parameter well above its critical value in the nondriven case, thus allowing the existence of stable Rabi oscillations in the presence of strong gain-loss situations. This is a consequence of the connection, found in our simulations, between the border of the parameter

space domain with real spectrum and the Rabi oscillation frequency between the noncentral wells of the TWP.

A consequence of extending regions with real spectrum using photon-assisted tunneling is the high sensitivity provided by the resonance phenomenon, which opens the door for applications such as sensors. In particular, detecting fluctuations in the chemical potential could be exploited in cold atom setups for sensing matter waves [63].

Finally, our three-level model could potentially be realized in experiments where photon-assisted tunneling occurs in the presence of a gain-loss controlled environment. An example of possible physical realization is with ultracold atoms trapped in optical lattices, which are coupled to a particle reservoir [30], and are subjected to the action of ac fields [9,11]. Another possibility is in a periodically modulated optical waveguide array. In this system, there is an analog of photon-assisted tunneling [15,16], which implemented in waveguides with balanced gain-loss [24] would allow to test our findings.

ACKNOWLEDGMENTS

L.M.-M. and E.A.-V. acknowledge financial support from Fondo Nacional de Desarrollo Científico y Tecnológico (FONDECYT) Grant No. 1190629.

-
- [1] P. K. Tien and J. R. Gordon, Multiphoton process observed in the interaction of microwave fields with the tunneling between superconductor films, *Phys. Rev.* **129**, 647 (1963).
 - [2] M. Grifoni and P. Hänggi, Driven quantum tunneling, *Phys. Rep.* **304**, 229 (1998).
 - [3] G. Platero and R. Aguado, Photon-assisted transport in semiconductor nanostructures, *Phys. Rep.* **395**, 1 (2004).
 - [4] B. J. Keay, S. J. Allen, J. Galan, J. P. Kaminski, K. L. Campman, A. C. Gossard, U. Bhattacharya, and M. J. M. Rodwell, Photon-assisted electric field domains and multiphoton-assisted tunneling in semiconductor superlattices, *Phys. Rev. Lett.* **75**, 4098 (1995).
 - [5] M. Glück, A. R. Kolovsky, and H. J. Korsch, Wannier-Stark resonances in optical and semiconductor superlattices, *Phys. Rep.* **366**, 103 (2002).
 - [6] L. P. Kouwenhoven, S. Jauhar, J. Orenstein, P. L. McEuen, Y. Nagamune, J. Motohisa, and H. Sakaki, Observation of photon-assisted tunneling through a quantum dot, *Phys. Rev. Lett.* **73**, 3443 (1994).
 - [7] T. H. Oosterkamp, L. P. Kouwenhoven, A. E. A. Koolen, N. C. van der Vaart, and C. J. P. M. Harmans, Photon sidebands of the ground state and first excited state of a quantum dot, *Phys. Rev. Lett.* **78**, 1536 (1997).
 - [8] S. Shapiro, Josephson currents in superconducting tunneling: The effect of microwaves and other observations, *Phys. Rev. Lett.* **11**, 80 (1963).
 - [9] A. Eckardt, T. Jinasundera, C. Weiss, and M. Holthaus, Analog of photon-assisted tunneling in a Bose-Einstein condensate, *Phys. Rev. Lett.* **95**, 200401 (2005).
 - [10] C. E. Creffield, and T. S. Monteiro, Tuning the Mott transition in a Bose-Einstein condensate by multiple photon absorption, *Phys. Rev. Lett.* **96**, 210403 (2006).
 - [11] N. Teichmann, M. Esmann, and C. Weiss, Fractional photon-assisted tunneling for Bose-Einstein condensates in a double well, *Phys. Rev. A* **79**, 063620 (2009).
 - [12] C. Weiss, and H. P. Breuer, Photon-assisted tunneling in optical lattices: Ballistic transport of interacting boson pairs, *Phys. Rev. A* **79**, 023608 (2009).
 - [13] Q.-T. Xie, S.-G. Rong, H.-H. Zhong, G.-B. Lu, and W.-H. Hai, Photon-assisted tunneling of a driven two-mode Bose-Einstein condensate, *Phys. Rev. A* **82**, 023616 (2010).
 - [14] C. Sias, H. Lignier, Y. P. Singh, A. Zenesini, D. Ciampini, O. Morsch, and E. Arimondo, Observation of photon-assisted tunneling in optical lattices, *Phys. Rev. Lett.* **100**, 040404 (2008).
 - [15] L. Li, X. Luo, X. Yang, M. Wang, X. Lu, and Y. Wu, An analog of photon-assisted tunneling in a periodically modulated waveguide array, *Sci. Rep.* **6**, 35744 (2016).
 - [16] L. Li, B. Wang and W. Li, Integer and fractional floquet resonances in a driven three-well system, *Photonics* **9**, 738 (2022).
 - [17] C. M. Bender and S. Boettcher, Real spectra in non-Hermitian Hamiltonians having PT symmetry, *Phys. Rev. Lett.* **80**, 5243 (1998).
 - [18] C. M. Bender, Making sense of non-Hermitian Hamiltonians, *Rep. Prog. Phys.* **70**, 947 (2007).
 - [19] N. Moiseyev, *Non-Hermitian Quantum Mechanics* (Cambridge University Press, London, 2011).
 - [20] K. G. Makris, R. El-Ganainy, D. N. Christodoulides, and Z. H. Musslimani, Beam dynamics in PT symmetric optical lattices, *Phys. Rev. Lett.* **100**, 103904 (2008).
 - [21] S. Longhi, Bloch oscillations in complex crystals with PT symmetry, *Phys. Rev. Lett.* **103**, 123601 (2009).
 - [22] A. Guo, G. J. Salamo, D. Duchesne, R. Morandotti, M. Volatier-Ravat, V. Aimez, G. A. Siviloglou, and D. N. Christodoulides,

- Observation of PT-symmetry breaking in complex optical potentials, *Phys. Rev. Lett.* **103**, 093902 (2009).
- [23] Y. D. Chong, L. Ge, and A. D. Stone, PT-symmetry breaking and laser-absorber modes in optical scattering systems, *Phys. Rev. Lett.* **106**, 093902 (2011).
- [24] C. E. Rüter, K. G. Makris, R. El-Ganainy, D. N. Christodoulides, M. Segev, and D. Kip, Observation of parity-time symmetry in optics, *Nat. Phys.* **6**, 192 (2010).
- [25] Z. Lin, H. Ramezani, T. Eichelkraut, T. Kottos, H. Cao, and D. N. Christodoulides, Unidirectional invisibility induced by PT-symmetric periodic structures, *Phys. Rev. Lett.* **106**, 213901 (2011).
- [26] L. Morales-Molina and S. A. Reyes, Non-adiabatic transitions in a non-symmetric optical lattice, *J. Phys. B: At. Mol. Opt. Phys.* **44**, 205403 (2011).
- [27] S. A. Reyes, F. A. Olivares, and L. Morales-Molina, Landau-Zener-Stückelberg interferometry in \mathcal{PT} -symmetric optical waveguides, *J. Phys. A: Math. Theor.* **45**, 444027 (2012).
- [28] A. Regensburger, M. A. Miri, C. Bersch, J. Nager, G. Onishchukov, D. N. Christodoulides, and U. Peschel, Observation of defect states in PT-symmetric optical lattices, *Phys. Rev. Lett.* **110**, 223902 (2013).
- [29] L. Feng *et al.*, Experimental demonstration of a unidirectional reflectionless parity-time metamaterial at optical frequencies, *Nat. Mater.* **12**, 108 (2013).
- [30] M. Kreibich, J. Main, H. Cartarius, and G. Wunner, Hermitian four-well potential as a realization of a PT-symmetric system, *Phys. Rev. A* **87**, 051601(R) (2013).
- [31] J. Wiersig, Enhancing the sensitivity of frequency and energy splitting detection by using exceptional points: Application to microcavity sensors for single-particle detection, *Phys. Rev. Lett.* **112**, 203901 (2014).
- [32] M. Wimmer *et al.*, Observation of optical solitons in PT-symmetric lattices, *Nat. Commun.* **6**, 7782 (2015).
- [33] T. Gao *et al.*, Observation of non-Hermitian degeneracies in a chaotic exciton-polariton billiard, *Nature (London)* **526**, 554 (2015).
- [34] Z. Zhang, Y. Zhang, J. Sheng, L. Yang, M. A. Miri, D. N. Christodoulides, B. He, Y. Zhang, and M. Xiao, Observation of parity-time symmetry in optically induced atomic lattices, *Phys. Rev. Lett.* **117**, 123601 (2016).
- [35] J. Doppler *et al.*, Dynamically encircling exceptional points in a waveguide: asymmetric mode switching from the breakdown of adiabaticity, *Nature (London)* **537**, 76 (2016).
- [36] H. Xu, D. Mason, L. Jiang, and J. G. E. Harris, Topological energy transfer in an optomechanical system with exceptional points, *Nature (London)* **537**, 80 (2016).
- [37] Y. Ashida, S. Furukawa, and M. Ueda, Parity-time symmetric quantum critical phenomena, *Nat. Commun.* **8**, 15791 (2017).
- [38] D. Leykam, K. Y. Bliokh, C. Huang, Y. D. Chong, and F. Nori, Edge Modes, Degeneracies, and topological numbers in non-Hermitian systems, *Phys. Rev. Lett.* **118**, 040401 (2017).
- [39] H. Hodaei *et al.*, Enhanced sensitivity at higher-order exceptional points, *Nature (London)* **548**, 187 (2017).
- [40] J. W. Yoon *et al.*, Time-asymmetric loop around an exceptional point over the full optical communications band, *Nature (London)* **562**, 86 (2018).
- [41] J. Zhang *et al.*, A phonon laser operating at an exceptional point, *Nature Photon* **12**, 479 (2018).
- [42] H. Zhao, Z. Chen, R. Zhao, and L. Feng, Exceptional point engineered glass slide for microscopic thermal mapping, *Nat. Commun.* **9**, 1764 (2018).
- [43] S. K. Özdemir, S. Rotter, F. Nori, and L. Yang, Parity-time symmetry and exceptional points in photonics, *Nat. Mater.* **18**, 783 (2019).
- [44] T. Yu, H. Yang, L. Song, P. Yan, and Y. Cao, Higher-order exceptional points in ferromagnetic trilayers, *Phys. Rev. B* **101**, 144414 (2020).
- [45] C. F. M. Faria and A. Fring, Time evolution of non-Hermitian Hamiltonian systems, *J. Phys. A: Math. Gen.* **39**, 9269 (2006).
- [46] C. F. M. Faria and A. Fring, Non-Hermitian Hamiltonians with real eigenvalues coupled to electric fields: From the time-independent to the time-dependent quantum mechanical formulation, *Laser Phys.* **17**, 424 (2007).
- [47] C. T. West, T. Kottos, and T. Prosen, PT-symmetric wave chaos, *Phys. Rev. Lett.* **104**, 054102 (2010).
- [48] J. Wu and X.-T. Xie, Jahn-Teller effect and driven binary oscillators in PT-symmetric potentials, *Phys. Rev. A* **86**, 032112 (2012).
- [49] S. Longhi, Dynamic localization and transport in complex crystals, *Phys. Rev. B* **80**, 235102 (2009).
- [50] N. Moiseyev, Crossing rule for a PT-symmetric two-level time-periodic system, *Phys. Rev. A* **83**, 052125 (2011).
- [51] R. El-Ganainy, K. G. Makris, and D. N. Christodoulides, Local PT invariance and supersymmetric parametric oscillators, *Phys. Rev. A* **86**, 033813 (2012).
- [52] X. Luo, J. Huang, H. Zhong, X. Qin, Q. Xie, Y. S. Kivshar, and C. Lee, Pseudo-parity-time symmetry in optical systems, *Phys. Rev. Lett.* **110**, 243902 (2013).
- [53] G. Della Valle and S. Longhi, Spectral and transport properties of time-periodic PT-symmetric tight-binding lattices, *Phys. Rev. A* **87**, 022119 (2013).
- [54] Y. N. Joglekar, R. Marathe, P. Durganandini, and R. K. Pathak, PT spectroscopy of the Rabi problem, *Phys. Rev. A* **90**, 040101(R) (2014).
- [55] T. E. Lee and Y. N. Joglekar, PT-symmetric Rabi model: Perturbation theory, *Phys. Rev. A* **92**, 042103 (2015).
- [56] X. Lian, H. Zhong, Q. Xie, X. Zhou, Y. Wu, and W. Liao, PT-symmetry-breaking induced suppression of tunneling in a driven non-Hermitian two-level system, *Eur. Phys. J. D* **68**, 189 (2014).
- [57] Y. Wu, B. Zhu, S.-F. Hu, Z. Zhou, and H. Zhong, Floquet control of the gain and loss in a PT-symmetric optical coupler, *Front. Phys.* **12**, 121102 (2017).
- [58] M. Chitsazi, H. Li, F. M. Ellis, and T. Kottos, Experimental realization of Floquet PT-symmetric systems, *Phys. Rev. Lett.* **119**, 093901 (2017).
- [59] Y. Luo *et al.*, Controlling stable tunneling in a non-Hermitian spin-orbit coupled bosonic junction, *New J. Phys.* **22**, 093041 (2020).
- [60] J. Li, A. K. Harter, Ji Liu, L. de Melo, Y. N. Joglekar, and L. Luo, Observation of parity-time symmetry breaking transitions in a dissipative Floquet system of ultracold atoms, *Nat. Commun.* **10**, 855 (2019).
- [61] M. De Carlo, F. De Leonardis, R. A. Soref, L. Colatorti, and V. M. N. Passaro, Non-Hermitian sensing in photonics and electronics: A review, *Sensors* **22**, 3977 (2022).

- [62] L. Morales-Molina and E. Arévalo, One-BEC-species coherent oscillations with frequency controlled by a second species atom number, *New J. Phys.* **24**, 013023 (2022).
- [63] L. Morales-Molina and E. Arévalo, Quantum sensing of matter waves using BEC oscillations, *Results Phys.* **41**, 105923 (2022).
- [64] R. Gati and M. K. Oberthaler, *J. Phys. B: At. Mol. Opt. Phys.* **40**, R61 (2007).
- [65] M. Albiez, R. Gati, J. Fölling, S. Hunsmann, M. Cristiani, and M. K. Oberthaler, A bosonic Josephson junction, *Phys. Rev. Lett.* **95**, 010402 (2005).
- [66] G. A. Watson, *Treatise on the Theory of Bessel Functions* (Cambridge University Press, Cambridge, England, 1994).